

experimental findings, we suggest that the continuous bombardment of the evolving film during the BEN process induces the further growth of the diamond embryo by preferential displacement and transformation of amorphous carbon to diamond at the interface between the two phases.

Under typical BEN conditions, the H<sub>2</sub> content in the plasma is >90 to 99%, so that each deposited carbon atom is bombarded by 20 to 200 H atoms. The energy transferred by the colliding H atoms (<1/3 of the H energy) is below the displacement energy of diamond of ~35 to 40 eV (25) but larger than that of graphite [~25eV (25)]. Even if the displacement efficiency of one H atom is low [~10% per 200 eV (16)], each graphitic atom will be displaced several times by the total number of the bombarding H atoms and imparted a considerable probability of occupying a diamond position. Further support for this picture of diamond growth in the bulk by transformation of a-C atoms at the diamond-a-C interface comes from our TEM (Fig. 1) and near edge x-ray absorption fine structure (NEXAFS) (8, 11) observations, which show that the diamond crystallites formed in BEN are always embedded in an a-C matrix and the diamond crystallite surface is never exposed in BEN. We could not find any evidence for diamond surface nucleation.

Once the diamond nucleus has reached a critical size, The BEN is stopped and the plasma is switched to nonbiased regular CVD conditions, in which the diamond crystallite grows via a CH<sub>3</sub>/C<sub>2</sub>H<sub>2</sub> radical surface growth mechanism (1-3), whereas the sp<sup>2</sup> bonded phases are etched by the harsh atomic hydrogen environment, exposing the buried perfect diamond crystallites for further growth. We have performed such a nonbiased CVD process for all the three sets of films reported here, and we have succeeded in growing polycrystalline diamond films.

The diamond crystallites that precipitate in the a-C:H matrix (sometimes on the graphitic edge, which serves as a nucleation site) are randomly oriented. Epitaxial growth is expected and observed for nucleation on Si steps, as established in our previous work (12). In this case, the epitaxy is a bulk process achieved through a "mold effect" (12, 15, 16), that is, the boundary conditions imposed by the crystalline structure of the Si step.

Previous attempts to understand diamond nucleation (9, 26-28) considered either gas phase or surface nucleation. Under BEN conditions, clusters that form on the surfaces or nucleate in the gas phase and stick to the surface are not likely to survive the harsh energetic bombardment. In contrast, a diamond nucleus precipitated in the bulk is stabilized and protected from the bombardment of energetic species.

Although this report specifically addresses diamond nucleation in BEN, it can be extended

to the nucleation of a host of metastable high-pressure phases of other materials. For example, all steps of our present model apply to the nucleation of cubic boron nitride (cBN) with energetic species, which is readily explained by the formation of cBN clusters in the matrix formed by subplantation (which includes edges of hexagonal BN planes). Similar to BEN of diamond, the cBN crystallites are always covered by a hexagonal BN layer and are never exposed on the surface (29), indicating their bulk precipitation nature.

References and Notes

1. J. C. Angus, C. C. Hayman, *Science* **241**, 643 (1988).
2. A. Paoletti, A. Tucciarone, Eds., *The Physics of Diamond*, Int. School of Physics, "Enrico Fermi" Course 135 (IOS Press, Amsterdam, 1997).
3. D. M. Gruen, I. Buckley-Golder Eds., *MRS Bull.* **23** (no. 9), 16 (1998).
4. F. P. Bundy, H. T. Hall, H. M. Strang, R. H. Wentroff, *Nature* **176**, 51 (1955).
5. J. Butler, H. Windischmann, *MRS Bull.* **23** (no. 9), 22 (1998).
6. S. Yugo, T. Kania, T. Kimura, T. Muto, *Appl. Phys. Lett.* **58**, 1036 (1991).
7. X. Jiang, C. P. Klages, R. Zachai, M. Hartweg, H. J. Fusser, *Appl. Phys. Lett.* **62**, 3438 (1993).
8. M. M. Garcia et al., *Appl. Phys. Lett.* **72**, 2105 (1998).
9. M. M. Garcia, I. Jimenez, O. Sanchez, C. Gomez-Alexandre, L. Vazquez, *Phys. Rev. B* **61**, 10383 (2000).
10. I. Gouzman, I. Lior, A. Hoffman, *Appl. Phys. Lett.* **72**, 296 (1998).
11. A. Hoffman, A. Heiman, S.H. Christiansen, *J. Appl. Phys.* **89**, 576 (2001).
12. S. T. Lee et al., *Science*, **287**, 104 (2000).
13. W. J. Zhang et al., *Phys. Rev. B* **61**, 5579 (2000).
14. W. R. Lambrecht et al, *Nature* **364**, 607 (1993).
15. Y. Lifshitz, S. R. Kasi, J. W. Rabalais, *Phys. Rev. Lett.* **62**, 1290, (1989).
16. \_\_\_\_\_, W. Eckstein, *Phys. Rev. B* **41**, 10468 (1990).
17. Y. Lifshitz, *Diam. Rel. Mater.* **8**, 1659 (1999).
18. Optimal BEN conditions are found by performing a subsequent 1-hour CVD growth step in which large

- diamond crystallites are formed and their maximal nucleation density (crystallites per cm<sup>2</sup>) can be determined.
19. G. Seifert, E. Eschrig, *Phys. Status Solidi* **127**, 573 (1985);
20. \_\_\_\_\_, W. Bieger, *Z. Phys. Chem.* **267**, 529 (1986),
21. D. Porezag, Th. Frauenheim, Th. Köhler, G. Seifert, R. Kaschner, *Phys. Rev. B* **51**, 12947 (1995).
22. J. Widany, F. Weich, Th. Köhler, D. Porezag, Th. Frauenheim, *Diam. Rel. Mater.* **5**, 1031 (1996).
23. M. M. M. Bilek, D. R. McKenzie, D. G. McCulloch, C. M. Goringe, *Phys. Rev. B* **62**, 3071 (2001). These ab initio simulations, performed to study a-C:H structure and not diamond nucleation, show the same trends as our calculations (a large coordination number, the formation of hydrogen-free sp<sup>3</sup> clusters, and H decoration of the cluster surface). These calculations independently verify our present data, but the small cell size (52 C atoms compared with 128 C atoms in our cell) does not allow observing large (27 C) diamondlike carbon clusters and inhibits the comparison of the C clusters to perfect diamond.
24. The reactivity of local structure was derived by Hartree-Fock calculations with a 3-21G basis set (30) and using a frontier orbital theory (31). The sites in the nanodiamond cluster where the HOMO (the highest occupied molecular orbital) is maximum have the highest reactivity for a carbon atom. The relaxation of the final hydrogen terminated structure was calculated by DFTB MD with the conjugated gradient approach.
25. F. Banhart, *Rep. Progr. Phys.* **62** 1181 (1999).
26. Y. Bar-Yam, T. D. Moustakas, *Nature* **342** 786 (1989).
27. P. Badziag, W. S. Verwoerd, W. P. Ellis, N. R. Greiner, *Nature* **343** 244 (1990).
28. N. M. Hwang, J. H. Hahn, D. Y. Yoon, *J. Cryst. Growth* **160** 87 (1996).
29. P. B. Mirkarimi, K. F. McCarty, D. L. Medlin, *Mater. Sci. Eng.* **R21**, 47 (1997).
30. J. S. Binkley, J. A. Pople, W. J. Hehre, *J. Am. Chem. Soc.* **102**, 939 (1980).
31. R. Hoffmann, *Rev. Mod. Phys.* **60**, 601 (1988).
32. Supported in part by the Research Grants Council of Hong Kong (grant 1051/00E), the Strategic Research Grants of City University of Hong Kong, and the Israeli Academy of Sciences.

Supporting Online Material  
[www.sciencemag.org/cgi/content/full/297/5586/1531/DC1](http://www.sciencemag.org/cgi/content/full/297/5586/1531/DC1)  
 SOM notes 1 to 6  
 References

31 May 2002; accepted 15 July 2002

## Oxidation-Resistant Gold-55 Clusters

H.-G. Boyen,<sup>1\*</sup> G. Kästle,<sup>1</sup> F. Weigl,<sup>1</sup> B. Koslowski,<sup>1</sup> C. Dietrich,<sup>1</sup> P. Ziemann,<sup>1</sup> J. P. Spatz,<sup>3</sup> S. Riethmüller,<sup>2</sup> C. Hartmann,<sup>2</sup> M. Möller,<sup>2</sup> G. Schmid,<sup>4</sup> M. G. Garnier,<sup>5</sup> P. Oelhafen<sup>5</sup>

Gold nanoparticles ranging in diameter from 1 to 8 nanometers were prepared on top of silicon wafers in order to study the size dependence of their oxidation behavior when exposed to atomic oxygen. X-ray photoelectron spectroscopy showed a maximum oxidation resistance for "magic-number" clusters containing 55 gold atoms. This inertness is not related to electron confinement leading to a size-induced metal-to-insulator transition, but rather seems to be linked to the closed-shell structure of such magic clusters. The result additionally suggests that gold-55 clusters may act as especially effective oxidation catalysts, such as for oxidizing carbon monoxide.

Bulk gold is oxidation-resistant in air even at elevated temperatures. Nonetheless, gold can react with oxygen. For example, Au<sub>2</sub>O<sub>3</sub> can be prepared electrochemically (1) or by exposure to highly reactive chemical environ-

ments such as ozone (2), atomic oxygen delivered by molecular dissociation at a hot filament (3), or radicals provided by an oxygen plasma (4-6).

Recently, it has been shown that the

## REPORTS

chemical properties of gold nanoparticles can differ from those of bulk gold. Ultrafine particles (clusters) with dimensions below 10 nm supported on thin oxide films such as SiO<sub>2</sub>, TiO<sub>2</sub>, or MgO exhibit extraordinary catalytic activity (7–10) in oxidation reactions such as oxidizing CO. In this specific case, a sharp maximum was observed in the catalytic activity at a particle size of about 3 nm that correlated with the opening of an energy gap in the electronic density of states at the Fermi level (8). Quantum size effects in the electronic structure caused by electron confinement to a restricted volume appeared to be responsible for the unexpected catalytic properties of the nanoscaled Au system.

We studied the size dependence of the oxidation behavior under exposure to oxygen atoms and radicals by depositing two different types of Au nanoparticles on silicon substrates covered by a thin layer of native silicon oxide. We used the self-organization of macromolecules to create inverse micelles for the preparation of nanoparticles with a reasonable small variation in particle size. We also used chemically stabilized closed-shell clusters [Au<sub>55</sub> clusters stabilized by a (PPh<sub>3</sub>)<sub>12</sub>Cl<sub>6</sub> ligand shell], which allowed us to deposit monodisperse Au particles.

We found that isolated Au<sub>55</sub> clusters show an extraordinary resistance to oxidation even if exposed to oxygen atoms and radicals as created in oxygen plasmas. Under identical conditions, bulk Au is readily oxidized into Au<sub>2</sub>O<sub>3</sub>. This unusual chemical property of clusters, however, cannot be attributed simply to a size-induced opening of an energy gap at the Fermi level  $E_F$ , because these clusters still exhibit metallic behavior. Also, both larger and smaller Au nanoparticles prepared by the micellar technique were oxidized under these conditions.

Briefly, the first preparation technique (11) exploits the self-assembly of diblock copolymers to inverse micelles in a nonpolar solvent such as toluene. After loading the core of the micelles with HAuCl<sub>4</sub>, monomicellar layers (with thickness corresponding to one micelle) could be obtained on top of native silicon oxide by dip coating. The polymer matrix was then removed by means of an oxygen plasma, resulting in an array of well-separated metallic nanoparticles of uniform size, which was controlled by adjusting the concentration of

the metal salt within the micellar solution.

The arrangement of these Au particles as measured by noncontact atomic force microscopy (AFM, in tapping mode) is shown in Fig. 1. Although not perfectly ordered, the particle arrangement exhibits a high degree of hexagonal short-range order, as evidenced by the corresponding autocorrelation function (inset, Fig. 1). From such AFM images, Gaussian size distributions with averages of  $7.9 \pm 1.2$  nm,  $2.9 \pm 0.5$  nm,  $1.6 \pm 0.3$  nm, and  $1.3 \pm 0.3$  nm could be extracted for the particles studied in this work.

During all preparational steps, the chemical state of the gold was determined by x-ray photoelectron spectroscopy (XPS) (12). We added a final hydrogen plasma step to ensure that the as-prepared nanoparticles were elemental gold without any detectable traces of oxides (<1%). Figure 2A shows the Au-4d binding energy region together with the C-1s and Cl-2s core lines, the latter representing the elements to be removed by the in situ plasma etching. After an appropriate etching time, the Cl signal completely vanished, and the C intensity decreased to below 0.005 monolayer (ML), which can be neglected in the context of the present work. Thus, isolated pure Au particles were available to study chemical interactions with reactive oxygen species.

Because of the small but finite size distribution of the Au particles prepared by the micellar technique, monodisperse Au<sub>55</sub> clusters (size 1.4 nm) stabilized by a PPh<sub>3</sub> ligand shell were also synthesized (13) and were deposited on native silica by spin coating from a CH<sub>2</sub>Cl<sub>2</sub> solution (14). Spin coating creates islands 1 ML in height after evaporation of the solvent on hydrophobic substrates (15). These samples were then exposed to an

oxygen plasma in order to remove the ligand shell (Fig. 2B), which allowed us to study the properties of “naked” Au<sub>55</sub> clusters.

Because we are interested in the response of such pure Au nanoparticles to highly reactive oxygen species as provided by an oxygen plasma (exposure for 10 min at 50 W and 0.005 mbar), a flat Au(111) surface was first treated under identical conditions for comparison to the bulk behavior. The corresponding XPS core-level spectra of the Au-4f region acquired for two different photoelectron take-off angles  $\phi$ , resulting in different surface sensitivities, are shown in Fig. 3A. Both spectra reveal four peaks originating from the metallic Au substrate (binding energies 84.0 and 87.7 eV) and Au bonded to oxygen (binding energies 85.8 and 89.5 eV). The oxide can be identified as Au<sub>2</sub>O<sub>3</sub> by the observed energy shift (4, 6). From the angular dependence of the different spectral weights, a surface oxide layer with a thickness of 2.9 nm (16) can be extracted. This corresponds to 0.7 nm of the original Au film, which is transformed into Au<sub>2</sub>O<sub>3</sub> during the plasma treatment.

Thus, when exposing small Au particles to such a plasma, we expect the formation of a core/shell system composed of an Au oxide shell and a pure Au core whose diameter should decrease with decreasing particle size. Finally, the oxidation of Au clusters should be complete for an initial size of 1.4 nm (two times 0.7 nm) and below. Hence, full oxidation is expected for clus-

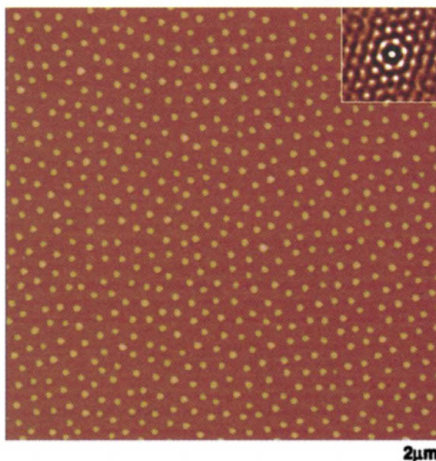


**Fig. 1.** AFM image of Au particles prepared by a micellar method (11) (z range, 20 nm). The inset shows the corresponding autocorrelation function indicating a high degree of hexagonal order. Analysis of the size distribution yields an average diameter of  $7.9 \pm 1.2$  nm.

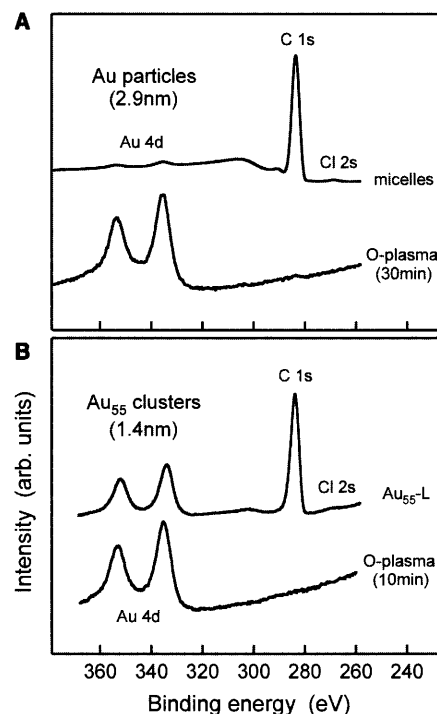


**Fig. 2.** Au-4d, C-1s, and Cl-2s core lines acquired from (A) HAuCl<sub>4</sub>-loaded micelles and (B) ligated Au<sub>55</sub> clusters supported on native silicon oxide before and after exposure to an in situ oxygen plasma. arb., arbitrary.

<sup>1</sup>Abteilung Festkörperphysik, <sup>2</sup>Abteilung Organische Chemie III, Universität Ulm, D-89069 Ulm, Germany. <sup>3</sup>Physikalisches Chemisches Institut, Universität Heidelberg, Im Neuenheimer Feld 253, D-69120 Heidelberg, Germany. <sup>4</sup>Institut für Anorganische Chemie, Universität GH Essen, Universitätsstrasse 5-7, D-45117 Essen, Germany. <sup>5</sup>Institut für Physik, Universität Basel, Klingelbergstrasse 82, CH-4056 Basel, Switzerland.

\*To whom correspondence should be addressed. E-mail: hans-gerd.boyen@physik.uni-ulm.de

## REPORTS

ters containing about 55 Au atoms and fewer.

The resulting chemical state can again be studied in detail by means of core-level spectroscopy, taking advantage of the well-defined spectroscopic fingerprint of the  $\text{Au}_2\text{O}_3$  compound. Figure 3B summarizes the Au-4f spectra, which were acquired for different particle sizes after the oxygen plasma treatment (under the same plasma conditions as in Fig. 3A). Starting with curve a, exposure of the 7.9-nm Au particles to oxygen atoms and radicals leads to the formation of two doublets that originate from elemental Au and from Au oxide, respectively. Quantitatively, from the spectral weights of the different components, the core radius as well as the shell width can be derived (17). This procedure yields a "surviving" metal core with a diameter of 6.5 nm for the plasma-treated sample, pointing to the transformation of a thin Au surface layer (thickness 0.7 nm) into Au oxide. These particles behave similarly to the Au film presented in Fig. 3A. Reducing the particle size to 2.9 nm (Fig. 3B, curve b) leads to a strongly lowered but still nonzero intensity of the metallic component. In this

case, the plasma treatment reduced the diameter of the elemental Au from 2.9 nm to 1.6 nm (again, a 0.65-nm Au layer transforms into Au oxide). Further reduction of the particle size to 1.6 nm and below should lead to a practically complete oxidation of the Au dots. However, the reduction of the particle size to 1.6 nm (curve c) actually leads to a dramatic increase in the spectral weight of the metallic component, evidencing an increased resistance against oxidation of these particles. This resistance is even more pronounced in the case of naked  $\text{Au}_{55}$  clusters (curve d, size 1.4 nm), which reveal a vanishing oxide contribution to the spectrum. We want to point out that in the latter two cases, all of the Au atoms forming a particle contribute to the XPS spectrum, because the electron mean free paths exceed the particle dimensions. If the initial particle size is further reduced to 1.3 nm and below (curves e and f), the peaks due to the photoemission from elemental Au are continuously damped. For the smallest particles investigated (<1 nm), the dominant photoemission arises from the oxide, which again points to an oxidation behavior

similar to that observed for bulk material.

Therefore, both types of Au particles studied here consistently demonstrate that the magic-number  $\text{Au}_{55}$  clusters show a maximum resistance against oxidation even if exposed to highly reactive oxygen species, thus making these clusters even nobler than bulk Au. It has to be emphasized that the first plasma treatment, which completely removed the ligand shell, did not lead to significant agglomeration of the bare  $\text{Au}_{55}$  clusters. Otherwise, larger particles would have formed, leading to a significant Au oxide contribution to the Au-4f spectrum according to Fig. 3B.

Coalescence between individual  $\text{Au}_{55}$  clusters during plasma-induced stripping of the ligand shell was actually found in the case of multilayered samples, which were prepared not by spin coating but simply by depositing a small droplet of the cluster solution onto a silicon wafer. After the evaporation of the solvent, a thickness of at least three layers of ligated  $\text{Au}_{55}$  clusters could be deduced. As can be seen in Fig. 3C, in this specific case the removal of the ligands by an oxygen plasma clearly caused the formation of gold oxide as expected for (agglomerated) Au particles larger than 1.4 nm, thereby giving additional evidence for the extraordinary stability of (separated)  $\text{Au}_{55}$  clusters against atomic oxygen.

An increased stability against molecular oxygen has been reported for free Al cluster anions corresponding to electronic closed-shell configurations (18). In order to investigate whether electronic properties (such as the opening of an energy gap) or structural properties (such as an atomic closed-shell structure) are responsible for the extraordinary stability of  $\text{Au}_{55}$  clusters, the valence band structure of the naked particles was determined after several plasma cycles, which reproducibly proved the enhanced nobleness of the clusters.

The resulting spectrum is presented in Fig. 4, together with the electronic structure of a clean Au film and of the  $\text{Au}_2\text{O}_3$  compound (6), respectively, serving as references for the naked  $\text{Au}_{55}$  particles. Taking the positions of the characteristic Au-5d features as a criterion, good overall agreement is found between the spectra obtained from the clusters and the Au bulk material, respectively. Most important, the existence of a steplike intensity at the Fermi level  $E_F$  (dotted line in Fig. 4) shows that bare clusters already form a metallic system similar to the case of  $\text{PPh}_3$ -ligated clusters (19). This finding is supported by comparison with the spectrum measured on Au oxide, which reveals significantly differing spectral features combined with a semiconducting behavior due to the opening of an energy gap at  $E_F$  (6).

Therefore, we conclude that the extraordinary chemical stability of  $\text{Au}_{55}$  is not

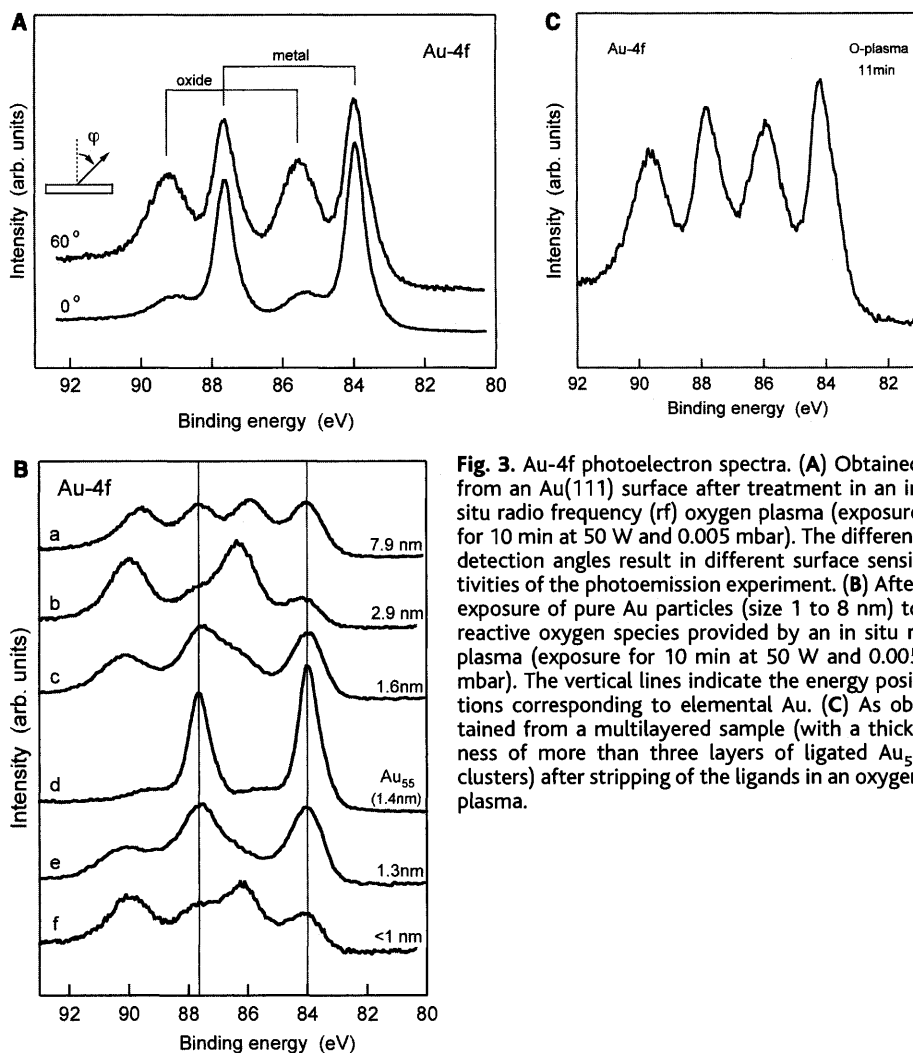


**Fig. 3.** Au-4f photoelectron spectra. (A) Obtained from an Au(111) surface after treatment in an in situ radio frequency (rf) oxygen plasma (exposure for 10 min at 50 W and 0.005 mbar). The different detection angles result in different surface sensitivities of the photoemission experiment. (B) After exposure of pure Au particles (size 1 to 8 nm) to reactive oxygen species provided by an in situ rf plasma (exposure for 10 min at 50 W and 0.005 mbar). The vertical lines indicate the energy positions corresponding to elemental Au. (C) As obtained from a multilayered sample (with a thickness of more than three layers of ligated  $\text{Au}_{55}$  clusters) after stripping of the ligands in an oxygen plasma.

## REPORTS

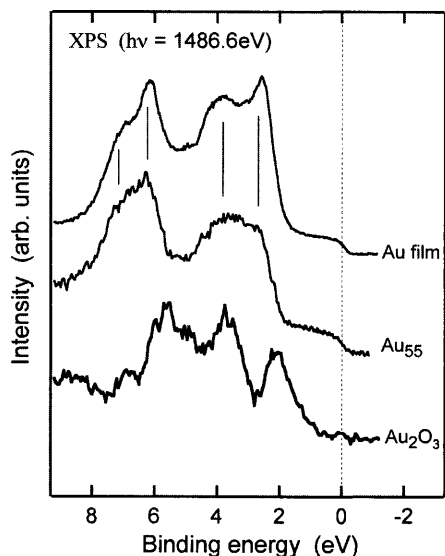


**Fig. 4.** XPS valence band spectra of naked  $Au_{55}$  clusters supported on silicon oxide, together with the corresponding spectra measured from an Au film and the  $Au_2O_3$  compound (6), respectively.

caused by size-induced modifications in the electronic structure. Rather, the closing of the second atomic shell is a more likely origin for the increased chemical stability. "Chemical selection," which avoids having an arbitrary number of atoms in a particle during the formation of phosphine-based Au clusters ( $Au_{13}$ ,  $Au_{55}$ ,  $Au_{147}$ , etc.), might itself result in oxidation resistance. On the other hand, the chemical stability of  $Au_{55}$  clusters might also be influenced by a high density of defects in the supporting material caused by the initial oxygen plasma treatment to remove the ligand shell. Defects in the support are known to modify the reactivity of Au clusters as compared to that of clusters on perfect substrates (7).

The observed stability against oxidation does not reflect a general property of ultrafine Au particles for particle diameters below a certain threshold. Rather, a nonmonotoneous size dependence was found with a pronounced minimum of reactivity for a cluster size of 1.4 nm. Interestingly enough, such a minimum of reactivity with atomic oxygen coincides with the existence of a pronounced maximum of catalytic efficiency for oxidation of CO to  $CO_2$  (8). Thus, we may speculate that  $Au_{55}$  clusters also exhibit unusual catalytic properties, such as in the oxidation of CO, because the catalyzing clusters will not be affected by the presence of atomic oxygen during the catalytic reaction.

### References and Notes

1. M. Peuckert, F. P. Coenen, H. P. Bonzel, *Surf. Sci.* **141**, 515 (1984).
2. D. H. Parker, B. E. Koel, *J. Vac. Sci. Technol. A* **8**, 2585 (1990).
3. D. D. Eley, P. B. Moore, *Surf. Sci.* **76**, L599 (1978).

4. J. J. Pireau, M. Liehr, P. A. Thiry, J. P. Delrue, R. Caudano, *Surf. Sci.* **141**, 221 (1984).
5. H. Ron, I. Rubinstein, *Langmuir* **10**, 4566 (1994).
6. B. Koslowski et al., *Surf. Sci.* **475**, 1 (2001).
7. U. Heiz, W.-D. Schneider, *J. Phys. D Appl. Phys.* **33**, R85 (2000).
8. M. Valden, X. Lai, D. W. Goodman, *Science* **281**, 1647 (1998).
9. M. Haruta, *Catal. Today* **36**, 153 (1997).
10. C. R. Henry, *Surf. Sci. Rep.* **31**, 231 (1998).
11. J. P. Spatz et al., *J. Lumin.* **76/77**, 168 (1998).
12. All photoemission experiments were carried out in a FISON ESCALAB-210 electron spectrometer, allowing in situ preparation and analysis by means of monochromatized Al-K $\alpha$  radiation (photon energy  $h\nu = 1486.6$  eV).
13. G. Schmid *Inorg. Synth.* **7**, 214 (1990).
14. Although other small gold clusters (such as  $Au_{13}$ ) have been reported, only  $Au_{55}$  appears to be readily synthesized in sufficient yield for studies such as these.
15. G. Radu, U. Memmert, U. Hartmann, *Proc. Spring Meet. German Phys. Soc. (Hamburg) Verhandl. DPG (VI)* **36**, 393 (2001).
16. The thickness of the surface oxide can be estimated within an analysis using Doniach-Sunjic line shapes (20) to model the different contributions to the spectra (27) and applying standard formulas for angle-resolved photoemission (22). Taking estimated mean free path values for the Au-4f photoelectrons

of 2.0 and 3.1 nm (23) and known density values of  $19.3$  g  $cm^{-3}$  and  $11$  g  $cm^{-3}$  for the pure Au metal and the  $Au_2O_3$  compound, respectively, a thickness of 2.9 nm can be extracted for the oxide layer from Fig. 3A, in agreement with previous experiments on ex situ plasma-oxidized Au films (6).

17. The nanoparticle is divided into a large number of identical cells, each contributing to the photoelectron current an intensity that is affected by the attenuation in cells being closer to the surface according to the mean free path of the corresponding material within these cells (Au and  $Au_2O_3$ ).
18. R. E. Leuchtner, A. C. Harms, J. A. W. Castleman, *J. Chem. Phys.* **91**, 2753 (1989).
19. H.-G. Boyen et al., *Phys. Rev. Lett.* **87**, 276401 (2001).
20. S. Doniach, M. Sunjic, *J. Phys. C* **3**, 385 (1970).
21. G. K. Wertheim, S. B. DiCenzo, *J. Electron. Spectrosc.* **37**, 57 (1985).
22. B. L. Henke, *Phys. Rev. A* **6**, 94 (1972).
23. M. P. Seah, W. A. Dench, *Surf. Interface Anal.* **1**, 2 (1979).
24. Financial support by the Bundesministerium für Bildung und Forschung, the Deutsche Forschungsgemeinschaft within SFB 569 and SPP 1072, the Swiss National Science Foundation, and the National Center of Competence in Research "Nanoscale Science" is gratefully acknowledged.

17 July 2002; accepted 25 July 2002

## Nanoparticles with Raman Spectroscopic Fingerprints for DNA and RNA Detection

YunWei Charles Cao, Rongchao Jin, Chad A. Mirkin\*

Multiplexed detection of oligonucleotide targets has been performed with gold nanoparticle probes labeled with oligonucleotides and Raman-active dyes. The gold nanoparticles facilitate the formation of a silver coating that acts as a surface-enhanced Raman scattering promoter for the dye-labeled particles that have been captured by target molecules and an underlying chip in microarray format. The strategy provides the high-sensitivity and high-selectivity attributes of gray-scale scanometric detection but adds multiplexing and ratioing capabilities because a very large number of probes can be designed based on the concept of using a Raman tag as a narrow-band spectroscopic fingerprint. Six dissimilar DNA targets with six Raman-labeled nanoparticle probes were distinguished, as well as two RNA targets with single nucleotide polymorphisms. The current unoptimized detection limit of this method is 20 femtomolar.

A highly sensitive and selective detection format for DNA relies on oligonucleotide-functionalized nanoparticles as probes, a particle-initiated Ag developing technique for signal enhancement, and a flatbed scanner for optical readout (1). The documented detection limit for this "scanometric DNA detection" format is 50 fM, (1) and the utility of the system has been demonstrated with short synthetic strands, polymerase chain reaction products, and genomic DNA targets (2, 3). However, a limitation of this approach is that

it is inherently a one-color system based on gray scale. The flexibility and applicability of all DNA-detection systems benefit from access to multiple types of labels with addressable and individually discernable labeling information. In the case of fluorescence, multiple fluorophores, including quantum dots, can be used to prepare encoded structures with optical signatures that depend on the types of fluorophores used and their signal ratio within the probes (4, 5). These approaches typically use micrometer-sized probes to obtain encoded structures with the appropriate signal intensities and uniformities. In the case of molecular fluorophores, overlapping spectral features and nonuniform fluorophore photobleaching rates lead to several potential complications (4, 6, 7).

Department of Chemistry and Institute for Nanotechnology, Northwestern University, 2145 Sheridan Road, Evanston, IL 60208, USA.

\*To whom correspondence should be addressed: camirkin@chem.northwestern.edu